Determination of the Contribution of the Myristoyl Group and Hydrophobic Amino Acids of Recoverin on its Dynamics of Binding to Lipid Monolayers

Philippe Desmeules,* Sara-Édith Penney,* Bernard Desbat,[†] and Christian Salesse*

*Unité de Recherche en Opthalmologie, Centre Hospitalier Universitaire de Québec, Pavillon CHUL, and Département d'Opthalmologie, Faculté de Médecine, Université Laval, Québec, Canada; and [†]Laboratoire de Physico-Chimie Moléculaire, UMR 5803 du Centre National de la Recherche Scientifique, Université Bordeaux I, Talence, France

ABSTRACT   It has been postulated that myristoylation of peripheral proteins would facilitate their binding to membranes. However, the exact involvement of this lipid modification in membrane binding is still a matter of debate. Proteins containing a Ca^{2+}-myristoyl switch where the extrusion of their myristoyl group is dependent on calcium binding is best illustrated by the Ca^{2+}-binding recoverin, which is present in retinal rod cells. The parameters responsible for the modulation of the membrane binding of recoverin are still largely unknown. This study was thus performed to determine the involvement of different parameters on recoverin membrane binding. We have used surface pressure measurements and PM-IRRAS spectroscopy to monitor the adsorption of myristoylated and nonmyristoylated recoverin onto phospholipid monolayers in the presence and absence of calcium. The adsorption curves have shown that the myristoyl group and hydrophobic residues of myristoylated recoverin strongly accelerate membrane binding in the presence of calcium. In the case of nonmyristoylated recoverin in the presence of calcium, hydrophobic residues alone are responsible for its much faster monolayer binding than myristoylated and nonmyristoylated recoverin in the absence of calcium. The infrared spectra revealed that myristoylated and nonmyristoylated recoverin behave very different upon adsorption onto phospholipid monolayers. Indeed, PM-IRRAS spectra indicated that the myristoyl group allows a proper orientation and organization as well as faster and stronger binding of myristoylated recoverin to lipid monolayers compared to nonmyristoylated recoverin. Simulations of the spectra have allowed us to postulate that nonmyristoylated recoverin changes conformation and becomes hydrated at large extents of adsorption as well as to estimate the orientation of myristoylated recoverin with respect to the monolayer plane. In addition, adsorption measurements and electrophoresis of trypsin-treated myristoylated recoverin in the presence of zinc or calcium demonstrated that recoverin has a different conformation but a similar extent of monolayer binding in the presence of such ions.

INTRODUCTION

Peripheral membrane proteins present highly complex interactions with membranes. The physical state of phospholipids, their headgroup, and the ionic strength of the solvent are some of the numerous parameters implicated in the membrane binding of these particular proteins (for reviews, see (1,2)). Moreover, intrinsic properties of these proteins can also influence their membrane binding. For example, binding of nucleotides and ions as well as acylation such as N-myristoylation are important features of peripheral proteins involved in membrane binding (3–6). N-myristoylation consists in the covalent attachment of a myristic acid to an N-terminal glycine residue of a protein via an amide linkage (7). It is now widely demonstrated that many viral and cellular proteins are N-terminally acylated by myristic acid (C14:0) and other fatty acids (i.e., C12:0, C14:1, C14:2, C16:0) (for reviews, see (8–10)). Such a hydrophobic modification has been shown to play a key role in protein targeting, protein-protein interaction, and/or in protein binding to membranes. In some cases, ligands like GTP, phosphate, or Ca^{2+} are involved in the modulation of membrane binding

of such proteins by controlling the orientation of the myristoyl moiety relative to the protein (for reviews, see (11–13)). In these cases, myristoyl groups constitute the so-called myristoyl switch. So far, the most studied one is the Ca^{2+}-myristoyl switch of recoverin.

Recoverin is a 23 kDa calcium-binding protein present in retinal rod cells of vertebrates (14) and is involved in the visual phototransduction cascade. Moreover, recoverin was identified as a cancer-retina antigen (for a review, see 15). This peripheral membrane protein contains four EF-hand motifs, a helix-loop-helix of 29 residues arranged to coordinate Ca^{2+}, but only two of them (EF-2 and EF-3) are able to bind Ca^{2+} (16–18). Recoverin is N-acylated predominantly by an amino-terminal myristoyl group (19–21) and acts as a calcium sensor by regulating the rod cell response to the fall in intracellular Ca^{2+} upon photoactivation of rhodopsin. Indeed, recoverin prevents the phosphorylation of rhodopsin by inhibiting rhodopsin kinase in a calcium-dependent manner (22–27). In the dark, the binding of two Ca^{2+} ions by recoverin induces the extrusion of its myristoyl group which increases its affinity for natural or model membranes (5,16,28–30) and for the peripheral membrane protein rhodopsin kinase. However, in the presence of light, the dissociation of Ca^{2+} from recoverin results in the sequestration of its myristoyl group in a hydrophobic cleft (17,31,

32). Permyakov et al. (33) have shown that recoverin binds a zinc ion at a site distinct from the calcium-binding sites. Moreover, like calcium ions, binding of zinc by recoverin increases its affinity for membranes (33).

Only few studies have been performed on the partitioning of acylated proteins in bilayers. Free-energy data for small myristoylated peptides (34) and for an acylated protein (35) have shown that a myristoyl moiety is barely enough (or not sufficient) to anchor a protein to membranes. Indeed, other contributions by the protein arising from charged residues (for a review, see (36)), conformational and mass-dependent entropy (37,38), steric effects, and hydrophobic residues (3) can be involved in the binding of acylated proteins to membranes. The intricate interaction of recoverin with membranes is still not well understood and minor protein contributions to membrane binding arising from amino acids has not been totally excluded or explored.

Monomolecular films, better known as Langmuir monolayers, are very useful to mimic biological membranes. Moreover, the continuous development of new surface-sensitive techniques (microscopy, infrared spectroscopy, synchrotron x ray, rheology, etc.) allows to probe the structure, dynamics, and organization of phospholipids, proteins, and other molecules at the air/water interface (for reviews, see 39–41). One of the powerful noninvasive techniques to investigate in situ monomolecular layers at the air water interface is polarization modulation infrared reflection absorption spectroscopy (PM-IRRAS). This method overcomes the water absorption limitation using rapid polarization modulation of the incident beam which allows the observation of infrared absorption bands of phospholipids and proteins at the monomolecular level (42,43). Furthermore, it is possible to extract information from the infrared spectra on conformation and orientation of molecules such as peptides and phospholipids present at the air/water interface (6,44–52) as well as the kinetics of hydrolysis of monolayers by enzymes (53–56).

Herein, we present the first study of the interaction of recoverin with phospholipid monolayers. Surface pressure and PM-IRRAS spectroscopy measurements have been used to probe the kinetics and the dynamics of adsorption of myristoylated and nonmyristoylated recoverin onto phospholipid monolayers in the presence and in the absence of calcium. In addition, protein adsorption measurements and limited proteolysis of recoverin in the presence of zinc have also been performed. This study reveals that recoverin presents a highly complex interaction with phospholipid monolayers involving its myristoyl moiety but also hydrophobic amino acids. Furthermore, nonmyristoylated recoverin can also bind phospholipid monolayers but its dynamics of binding differs very much from that of the myristoylated protein. Finally, binding of zinc by recoverin induces a conformational change different from that of calcium although similar extents of adsorption are obtained in the presence of these ions.

MATERIALS AND METHODS

Materials

The deionized water used for the preparation of buffer solutions was highly purified with a NANOpure purification apparatus (Barnstead, Dubuque, IA). This water had a resistivity of no less than 18.2 MΩ*cm and a surface tension of 72 ± 0.1 mN/m at room temperature. Ultrapure NaCl (99.9%) was purchased from J. T. Baker (Phillipsburg, NJ). HEPES (n-[2-hydroxy-ethyl])piperazine-n′-[2-ethane sulfonic acid]) (99.5%), 2-mercaptoethanol, $ZnCl_2$, phenylmethylsulfonyl fluoride, and ethylene-glycol-bis-(β-aminoethyl ether) N,N′-tetra acetic acid (EGTA) were from Sigma (St. Louis, MO). $CaCl_2$, $CHCl_3$ (99.9%) and deuterated water (99,9%) were purchased from Fluka (Neu-Ulm, Germany), Omega (Lévis, Canada), and Euriso-top (Saint-Aubin, France), respectively.

Preparation and cloning of recoverin cDNA

Total RNA from freshly dissected bovine (*Bos Taurus*) retina has been isolated by the Tri-reagent method (Sigma) and used for reverse-transcription reaction (RevertAid H Minus First Strand cDNA Synthesis Kit, Fermentas, Burlington, Ontario, Canada). Then, first strand cDNA was used as a template for PCR using primers designed to amplify the coding sequence of the bovine recoverin gene (M95858) and to introduce *Nde*I and *Bam*HI restriction sites. The full-length bovine cDNA of recoverin has then been ligated into the pET11a plasmid (Novagen, Madison, WI) to generate the pET11a-recoverin expression vector (pET11a-Rec).

Expression and purification of myristoylated and nonmyristoylated recombinant recoverin

Nonmyristoylated and myristoylated recoverin were expressed and purified essentially as reported by Ray et al. (57) and modified by Desmeules et al. (58). Briefly, myristoylated recoverin was expressed in *E. coli* strain BL21 (DE3) pLysS (Novagen) transformed with the pET11a-Rec vector and a vector encoding for *N*-myristoyl-transferase (pBB131, kindly provided by Dr. James B. Hurley, University of Washington, Seattle). The bacteria were grown in LB medium at 37°C containing ampicillin (100 μg/ml) and kanamycin (50 μg/ml). To achieve myristoylation of recoverin, an aqueous solution of sodium myristate (0.08 mM) final concentration was added to the culture medium 20 min before the induction of protein expression (7,58). Nonmyristoylated recoverin has been overexpressed as described for myristoylated recoverin but in the absence of sodium myristate. After preparation of the cleared lysate, myristoylated or nonmyristoylated recoverin have been purified by a single-step procedure using the calcium-dependent binding of recoverin to low-substituted phenyl Sepharose (58). The eluted fractions containing recoverin were aliquoted and frozen at −70°C until use.

Determination of the concentration of purified recoverin and its myristoylation level

The purity of recoverin was at least 99% as judged by gel electrophoresis and Coomassie blue staining. Protein concentration was determined for each eluted fraction using the Bradford method (59) with bovine serum albumin as the protein standard. Myristoylation of recoverin has been quantified by reverse-phase high pressure liquid chromatography using a hydrophobic column Jupiter 5μ C4 300 Å (Phenomenex, Torrance, CA). Briefly, purified recoverin was dialyzed against buffer A (5 mM HEPES, pH 7.5, 100 mM NaCl, 5 mM β-mercaptoethanol, and 1 mM $CaCl_2$). Then, 0.1% of trifluoroacetic acid was added before injection of the purified protein onto the hydrophobic column. Retention time for myristoylated recoverin was 4 min longer than for nonmyristoylated recoverin when using a 0–80% acetonitrile gradient containing 0.1% trifluoroacetic acid (58). Protein elution was monitored by UV absorption and determination of the peak area allowed us

to estimate that fractions of myristoylated recoverin used in our experiments were no less than 97% myristoylated.

Protein adsorption measurements in monolayers and data analysis

A home-built trough (50 cm^2) made of glass or a multiwell glass plate (Kibron, Helsinki, Finland) were filled with 20 ml (or 0.5 ml for the multiwell glass plate) of HEPES buffer containing either calcium or zinc (1 mM HEPES, pH 7.5, 100 mM NaCl, 1 mM β-mercaptoethanol, 1 mM CaCl$_2$, or 1 mM ZnCl$_2$) or in the absence of divalent ions (1 mM HEPES, pH 7.5, 100 mM NaCl, 1 mM β-mercaptoethanol, and 1 mM EGTA). The trough used in our experiments was made of glass because no adsorption was observed at the air/water interface when using Teflon-covered troughs due to the irreversible binding of recoverin to this hydrophobic material. Buffers were cleaned before each experiment from any surfactants by compression of the interface followed by suction until no change in surface pressure (Π) was detected. Then, the phospholipid monolayer was formed by spreading a few microliters of a chloroform solution of dimyristoyl-phosphatidylcholine (DMPC) (Avanti Polar Lipids, Alabaster, AL) at the air-water interface using a microsyringe (Hamilton, Reno, NV) until the desired surface pressure (Π_0) was reached. The surface pressure (Π) was measured by the Wilhelmy method using a microbalance (Riegler and Kirstein, Potsdam, Germany; or Nima Technology, Coventry, UK) connected to a computer. Recoverin was injected into the subphase using a microsyringe and the surface pressure was monitored during its adsorption onto the DMPC monolayer at 21°C. The subphase was not stirred and thus the kinetics of adsorption of recoverin was solely due to self-diffusion of the protein. The surface pressure increase ($\Delta\Pi$) after the injection of recoverin corresponds to Π_∞-Π_0, which are, respectively, the surface pressure at the equilibrium and the initial surface pressure. The values of surface pressure versus time recorded during the adsorption of recoverin onto phospholipid monolayers were fitted using the following stretched exponential equation adapted to surface pressure measurements by Pitcher et al. (60),

$$\Pi_t = \Pi_\infty - \Pi_0 e^{-(kt)^\beta}, \qquad (1)$$

where Π_t is the surface pressure of the monolayer at time t, Π_∞ is the surface pressure of the monolayer at equilibrium, Π_0 is the initial surface pressure of the monolayer, k is the rate coefficient, and β is the exponential scaling factor.

Monitoring of the adsorption of recoverin to phospholipid monolayers by PM-IRRAS spectroscopy

PM-IRRAS combines Fourier transform mid-IR reflection spectroscopy with rapid polarization modulation of the incident beam (42,43,61). In fact, a photoelastic modulator generates alternating linear states of the polarized light into parallel (E_p) and perpendicular (E_s) radiations. The difference between the spectra of the sample at both polarization states is measured

$$\frac{\Delta R}{R} = \frac{(R_p - R_s)J_2(\Phi_0)}{(R_p + R_s) + (R_p - R_s)J_0(\Phi_0)}, \qquad (2)$$

where R_p and R_s are the reflectivity of the interface for polarized light, $J_0(\Phi_0)$ and Φ_0 are the zero- and second-order Bessel functions, whereas Φ_0 is the phase of the Bessel function related to variations of the modulation of polarization according to the wavelength. Moreover, to remove the isotropic contributions from bulk water and water vapor, experimental drifts and to get rid of the dependence on the Bessel function, the spectrum of the phospholipid monolayer in the presence of the adsorbed recoverin is divided by that of the phospholipid monolayer (or of the subphase) in the absence of protein to produce the resulting normalized PM-IRRAS spectrum:

$$\left(\frac{\Delta R}{R}\right)_{\text{norm}} = \left(\frac{(\Delta R/R)_{\text{film}}}{(\Delta R/R)_{\text{subphase}}}\right). \qquad (3)$$

The signal/noise ratio of the technique is therefore enhanced because water vapor molecules do not contribute to the PM-IRRAS signal. Each PM-IRRAS spectrum was the result of the co-addition of 600 scans at a resolution of 8 cm^{-1}. Consequently, a typical PM-IRRAS spectrum was obtained after ~9 min of acquisition. In PM-IRRAS experiments, two types of subphases were used: a water subphase buffered with HEPES (1 mM HEPES, pH 7.5, 100 mM NaCl, 1 mM β-mercaptoethanol, 1 mM CaCl$_2$) or a deuterated water (D$_2$O) subphase (1 mM HEPES, pD 7.9, 100 mM NaCl, 1 mM β-mercaptoethanol, CaCl$_2$ 1 mM). pD was adjusted according to the relation pD = pH + 0.4 using NaOD. The CaCl$_2$ used in this buffer was an anhydrous powder (Sigma). The trough was enclosed in a Plexiglas chamber to protect it from the dust. Moreover, for the experiments with D$_2$O subphase, the chamber was saturated with D$_2$O vapor to prevent the exchange of H$_2$O with the D$_2$O subphase during the experiments. For all measurements with the H$_2$O subphase except for those where measurements have been performed in the absence of a phospholipid monolayer, a polarizer selecting the R_p reflected light has been positioned in front of the detector as described earlier (62). This procedure was necessary because a rather weak amide I signal was obtained with this subphase without polarizer. In addition, in this case, the spectrum of the phospholipid-recoverin monolayer has been subtracted from that of the pure phospholipid monolayer.

Measurement of the infrared spectrum of recoverin in solution by attenuated total reflection spectroscopy

A drop (5 μl) of a solution of recoverin at a concentration of 2.5 μg/ml was deposited on the stage of the Golden Gate attenuated total reflection (ATR) accessory (Specac, Woodstock, NY) and the spectrum was measured. The spectrum of the buffer was subtracted from that of recoverin to get the spectrum of the pure protein.

Simulation of the PM-IRRAS spectra

Simulated spectra have been obtained using a general software program developed for modeling the reflectivity of absorbing layered systems (63) and extended to anisotropic systems using the matrix method of Berreman (64). To determine whether the decrease in intensity of the spectra of nonmyristoylated recoverin at large extents of adsorption can be explained by a hydration effect, simulations were performed where the optical constants of water were obtained from Bertie and Lan (65) and those of the peptide from Buffeteau et al. (66). In addition, simulations of the spectra of myristoylated recoverin have been performed to estimate its orientation with respect to the plane of the monolayer. The number of turns of each α-helix and the angle between each of these α-helices of recoverin and the z axis taken as 0° (see Fig. 1) have thus been estimated on the basis of its NMR structure (28). Then, using experimental values of amide I and II bandwidths of myristoylated recoverin, simulated spectra were generated using the same general software (63) where the optical constants have been modified to take into account the orientation and the size of each α-helix of recoverin.

Limited proteolysis of recoverin

TPCK-treated trypsin (USB, Cleveland, OH) (26 ng) was added to 2.6 μg of myristoylated recoverin in a final volume of 20 μl of buffer in the presence of CaCl$_2$ or ZnCl$_2$ (5 mM HEPES pH 7.4, 100 mM NaCl, 1 mM β-mercaptoethanol, and 1 mM CaCl$_2$ or 1 mM ZnCl$_2$). After 15 min, proteolysis was stopped by addition of phenylmethylsulfonyl fluoride and Laemmli sample buffer directly to the reaction tube. Then, proteolysis pattern was visualized by SDS-PAGE and Coomassie blue staining.
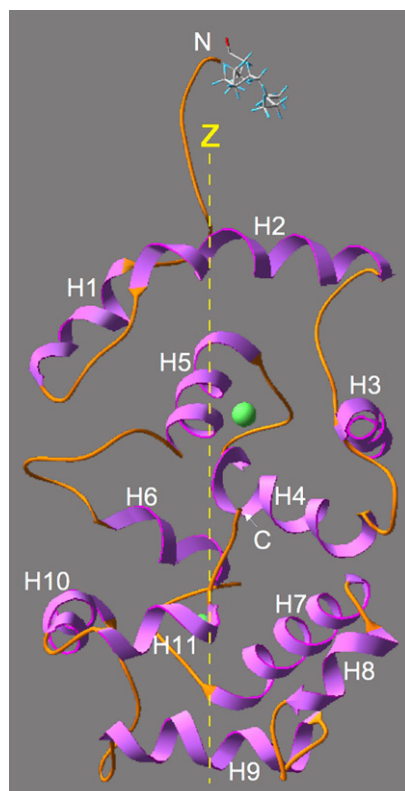
FIGURE 1 Structure of Ca^{2+}-bound myristoylated recoverin ((28); 1jsa.pdb). The α-helices have been labeled H1-H11. *C* and *N* represent the C- and N-terminal parts of recoverin. The myristoyl moiety can be seen at the N-terminal. The *z* axis of recoverin has been taken as the normal to α-helix 2 (H2). The two solid green circles correspond to the bound calcium ions.

RESULTS AND DISCUSSION

Adsorption of myristoylated and nonmyristoylated recoverin onto DMPC monolayers

Fig. 2 shows typical Π-t adsorption isotherms of myristoylated and nonmyristoylated recoverin onto a DMPC monolayer in the presence and the absence of calcium. It can be seen that the slowest kinetics of adsorption are observed in absence of calcium (in presence of EGTA). In the case of myristoylated recoverin, its adsorption in absence of calcium leads to a surface pressure increase from 5 to 12 mN/m within 6500 s. However, its adsorption is drastically accelerated by the presence of calcium ions, which leads to an increase of surface pressure from 6 to 16.5 mN/m within only 200 s (see *inset* of Fig. 2). The Π-t adsorption isotherm of the nonmyristoylated recoverin is also accelerated by the presence of calcium. However, the effect of calcium is smaller than in the case of myristoylated recoverin (see *inset* of Fig. 2). In fact, in the absence of calcium, nonmyristoylated recoverin adsorption leads to a surface pressure increase from 5 to 11.3 mN/m within 6500 whereas, in the presence of calcium, an increase
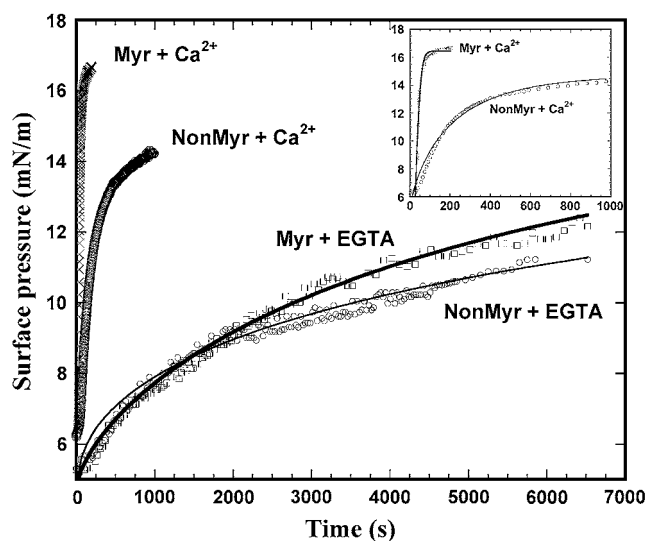

FIGURE 2 Typical Π-t adsorption isotherms of myristoylated (*Myr*) and nonmyristoylated (*NonMyr*) recoverin onto a DMPC monolayer ($\Pi_0 = 5$ mN/m) in the presence (Myr + Ca^{2+} and NonMyr + Ca^{2+}) or absence of calcium (Myr + EGTA and NonMyr + EGTA) into the subphase. The time zero corresponds to the injection of recoverin into the subphase. In all cases, the final concentration of recoverin was 50 nM. The subphase was: 1 mM HEPES, pH 7.5, 100 mM NaCl, and 1 mM $CaCl_2$ (or 1 mM EGTA). (*Inset*) To better appreciate the kinetics of adsorption of myristoylated (*Myr*) and nonmyristoylated (*NonMyr*) recoverin in presence of calcium, the *x* axis has been extended to 1000 s. These data are representative of three independent experiments.

from 6 to 14.5 mN/m within 1000 s is observed for recoverin in the absence of its myristoyl moiety. This result suggests that nonmyristoylated recoverin underwent a conformational change after calcium binding, exposing amino acids which increased its affinity for the phospholipid monolayer. The trend of these curves has been successfully fitted with a stretched exponential (Fig. 2), which allows us to quantify and compare the rate of adsorption of recoverin in these different conditions. Table 1 presents the rate coefficients calculated for myristoylated and nonmyristoylated recoverin in the presence and the absence of calcium. The rate-constant ratios indicate that the adsorption of myristoylated recoverin in the presence

TABLE 1 Rate constants obtained from the curve fitting of the adsorption curves (Fig. 2) using a stretched exponential (see Eq. 1) for myristoylated recoverin in the presence (Myr + Ca^{2+}) and the absence (Myr + EGTA) of calcium as well as for nonmyristoylated recoverin in the presence (NonMyr + Ca^{2+}) and the absence (NonMyr + EGTA) of calcium; the rate constant ratio (k_{Ca}^{2+} / k_{EGTA}) and the coefficient of correlation (*R*) are also presented

	Rate constant k (s^{-1})	Rate constant ratio (k_{Ca}^{2+} / k_{EGTA})	*R*
Myr + Ca^{2+}	0.028	165	0.990
Myr + EGTA	0.00017	—	0.993
NonMyr + Ca^{2+}	0.0048	25	0.995
NonMyr + EGTA	0.00019	—	0.987

of calcium is 165 times faster than in the absence of calcium whereas the adsorption of nonmyristoylated recoverin in the presence of calcium is 25 times faster than in the absence of calcium.

These results can be interpreted on the basis of the NMR and x-ray diffraction structural data obtained for myristoylated and nonmyristoylated recoverin in the presence and the absence of calcium (17,28,32). In the absence of calcium, the NMR study in solution has shown that the myristoyl group of calcium-free myristoylated recoverin is buried inside the protein in contact with a deep hydrophobic cleft formed by residues F23, W36, Y53, F56, F57, and Y86 (16,32). The presence of this hydrophobic cleft has also been demonstrated for the calcium-free nonmyristoylated recoverin by x-ray crystallography (17). Consequently, recoverin in its calcium-free state has less peripheral hydrophobic residues in contact with the solvent than the calcium-bound state. Indeed, it has been shown that Ca^{2+} binding to recoverin leads to the unclamping and extrusion of the myristoyl group but also to a 45° rotation of the N-terminal domain relative to the carboxy-terminal domain, thus exposing hydrophobic residues F23, W36, Y53, F56, F57, and Y86 to the solvent (28,29,67). Furthermore, NMR and circular dichroism studies have shown that nonmyristoylated recoverin undergoes a calcium-modulated structural change very similar to that of myristoylated recoverin upon calcium binding (28,29,68). These results corroborate the experimental observation that nonmyristoylated recoverin can be purified using Ca^{2+}-dependent binding to the hydrophobic phenyl Sepharose resin (57,58) with a yield comparable to the myristoylated form. The results presented in Fig. 2 thus suggest that the higher rate (25-fold, Table 1) of adsorption of nonmyristoylated recoverin onto phospholipid monolayers in the presence of calcium compared to the calcium-free nonmyristoylated recoverin can be explained by the interaction of the exposed hydrophobic region of recoverin with the monolayer in the presence of calcium. These data thus strongly suggest that the increased rate of adsorption of myristoylated recoverin compared to nonmyristoylated recoverin in the presence of calcium (0.028 s^{-1}/0.0048 s^{-1} ≈ 5.8-fold, Table 1) arises solely from the myristoyl moiety of recoverin. In others words, our results indicate that the increase in surface hydrophobicity of recoverin reduces the kinetics barrier of its adsorption to phospholipid monolayers. It has been previously observed that the rate of adsorption of proteins onto lipid monolayers increases with protein surface hydrophobicity (69–71). As suggested by Xia et al. (70) in their revised model of diffusion-controlled adsorption of trichosanthin, the higher the surface hydrophobicity of a protein, the higher its probability to collide the monolayer with an appropriate orientation which can allow it to remain stable at the lipid/water interface. In fact, the slower adsorption of myristoylated and nonmyristoylated recoverin in the absence of calcium could be explained by a slower stabilization of these calcium-free recoverins by phospholipid monolayers.

These measurements demonstrating the much slower binding of myristoylated recoverin in the absence of calcium compared to myristoylated recoverin in the presence of calcium contrasts with previous surface plasmon resonance (SPR) (72) and force spectroscopy (FS) (5) measurements. Indeed, SPR and FS did not allow us to observe binding of nonmyristoylated and calcium-free recoverin to lipid bilayers. This can be explained by the lower initial lateral pressure used in the present study compared to the higher lateral pressure of the supported bilayers used in the SPR (72) and FS (5) experiments and/or by the faster kinetics of these methods compared to protein binding onto lipid monolayers. Indeed, for example, in the FS experiments, the AFM tip covalently bound with recoverin was quickly approached to and removed from the lipid bilayer within 10 ms whereas saturation of the monolayer by myristoylated recoverin is achieved within 200 s (see Fig. 2). In our experiments, proteins thus have plenty of time to properly orient and organize to optimize binding. At higher surface pressures that approach lipid bilayer lateral pressures, recoverin binding cannot readily be observed by surface-pressure measurements, although protein binding could be still measured by infrared spectroscopy (results to be published elsewhere).

Monitoring of the adsorption of recoverin onto DMPC monolayers by PM-IRRAS spectroscopy

To obtain molecular information on the dynamics, orientation, and secondary structure of myristoylated and nonmyristoylated recoverin during their adsorption onto phospholipid monolayers, we have used PM-IRRAS at the air/water interface. Recoverin was injected into the subphase containing calcium and scan acquisition was started immediately to follow the kinetics of recoverin adsorption onto the DMPC monolayer. Typical spectra recorded during myristoylated recoverin adsorption that cause a surface pressure increase from 5 to 13 mN/m are presented in Fig. 3. Two broad bands are standing out in each spectrum corresponding, respectively, to the amide I (centered at 1655 cm^{-1}) and amide II (at ~1550 cm^{-1}) bands. The intensity of the amide I band increases with surface pressure. The amide I band is widely used to determine the secondary structure of proteins (73,74). The position of the amide I band (1655 cm^{-1}) of myristoylated recoverin in the presence of calcium reveals a major proportion of α-helices (49,75,76), which is in agreement with its known NMR structure in solution (Fig. 1) (28,32). Moreover, circular dichroism has shown that myristoylated as well as nonmyristoylated recoverin contains 65% α-helices (68).

Given that no infrared spectrum of recoverin in aqueous solution is available in the literature, ATR-FTIR spectra of myristoylated recoverin have been measured using the stage of the Golden Gate to obtain a spectrum of the protein in solution (see spectrum 6 in Fig. 3). The position of the amide I band (1646 cm^{-1}) together with the observation of an increased bandwidth on the low frequency part indicates
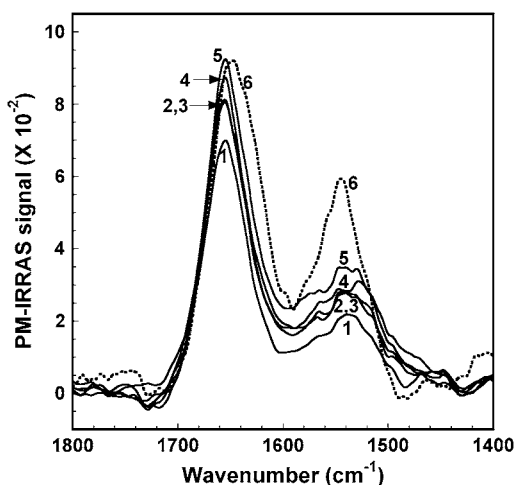
FIGURE 3 Typical PM-IRRAS spectra of myristoylated recoverin during its adsorption onto a DMPC monolayer in the presence of calcium ($\Pi_0 = 5$ mN/m). Each PM-IRRAS spectrum was obtained during the 9 min of acquisition: spectra 1 (5–11.2 mN/m; 0–9 min), 2 (11.5–12.7 mN/m; 10–18 min), 3 (12.7–12.8 mN/m; 19–27 min), 4 (12.8–12.9 mN/m; 28–36 min), and 5 (12.9–13 mN/m; 37–45 min). Spectrum 6 has been measured using the stage of the Golden gate with a drop (5 μl) of a solution of recoverin at a concentration of 2.5 μg/ml. The subphase was 1 mM HEPES, pH 7.5, 100 mM NaCl, and 1 mM CaCl$_2$. The final concentration of recoverin was 50 nM. These measurements were performed with a polarizer positioned in front of the detector as described earlier (62). These data are representative of two independent experiments.

disordering of recoverin secondary structure in solution compared to when it is bound to lipid monolayers. Moreover, it has been previously shown that information can be obtained on the orientation of an α-helical peptide from the measurement of the amide I/amide II ratio (44). The discrepancy between the ratio of the amide I/amide II bands observed in the ATR-FTIR spectrum (1.6; spectrum 6, Fig. 3) and that in the PM-IRRAS spectra (2.7; spectra 1–5, Fig. 3) suggests that recoverin has an anisotropic organization at the air/water interface in contrast to being randomly oriented in solution. Simulations of these spectra of recoverin have been performed (Fig. 4) to estimate its orientation by comparing the experimental amide I/amide II ratio with those of the simulated spectra. It can be seen that the spectrum with an amide I/amide II ratio that most closely corresponds to the experimental value of 2.7 (Fig. 3) is that where the Z axis of recoverin (Fig. 1) has an orientation of 0° (curve 1, Fig. 4). In fact, such a high amide I/amide II ratio suggests that most of the α-helices of recoverin are preferentially oriented parallel to the water surface, which fits well with the 0° orientation of the Z axis of recoverin shown in Fig. 1 and is in good agreement with the model proposed by Valentine et al. (67), who have estimated the orientation of myristoylated recoverin in bicelles.

Fig. 5 shows the PM-IRRAS spectra measured during the adsorption of nonmyristoylated recoverin onto a DMPC monolayer in the presence of calcium. It can be seen that the
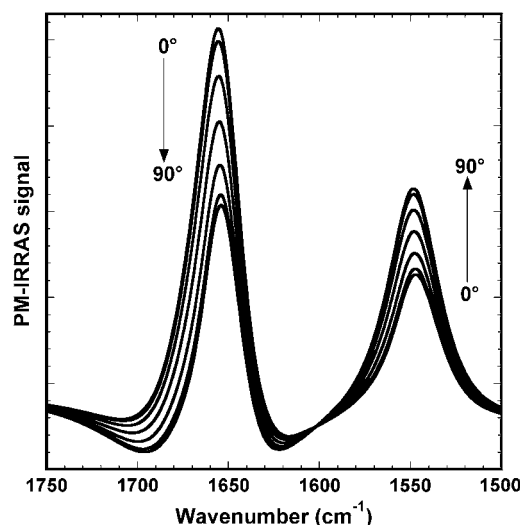

FIGURE 4 Simulated spectra of myristoylated recoverin at different orientations (from $\theta = 0$ to 90°) on the basis of its NMR structure (28). The z axis has been taken as the normal to α-helix 2 of recoverin (as well as several other α-helices). The orientation shown in Fig. 1 corresponds to $\theta = 0°$.

intensity of the amide I band of these spectra is weaker than those measured for myristoylated recoverin (compare Figs. 3 and 5). Normalized spectra of myristoylated and non-myristoylated recoverin after 36 min of adsorption have been compared in the inset of Fig. 5. It can be seen that the position and the width of the amide I band and the amide I/amide II ratio are almost exactly the same, which suggests that, up to this extent of adsorption, the organization of myristoylated and nonmyristoylated recoverin is the same when bound to lipid monolayers. However, from that point, the organization of the adsorbed nonmyristoylated recoverin changes drastically as can be seen in spectra 5 and 6 (Fig. 5). This effect is more clearly demonstrated when the intensity of the amide I band of the adsorbed myristoylated and non-myristoylated recoverin in the presence of calcium is plotted as a function of time (Fig. 6). It can be seen that 36 min after the injection of nonmyristoylated recoverin into the subphase, the amide I band intensity starts to decrease until a very weak intensity is reached in the last spectrum (after 54 min adsorption). In contrast, the amide I band intensity of myristoylated recoverin increases almost linearly from 9 to 45 min (Fig. 6). These PM-IRRAS spectra thus reveal that the dynamics and the temporal organization of myristoylated and nonmyristoylated recoverin in presence of calcium are completely different when adsorbed onto phospholipid monolayers after 36 min of adsorption.

The intensity of the PM-IRRAS signal is proportional to the number of molecules per surface unit and to the molecular conformation and orientation of the molecules at the air/water interface (61). In our experiments, measurements were performed at the same constant area for both myristoylated and nonmyristoylated recoverin and the same amount of recoverin was injected into the subphase. Thus, the reduction
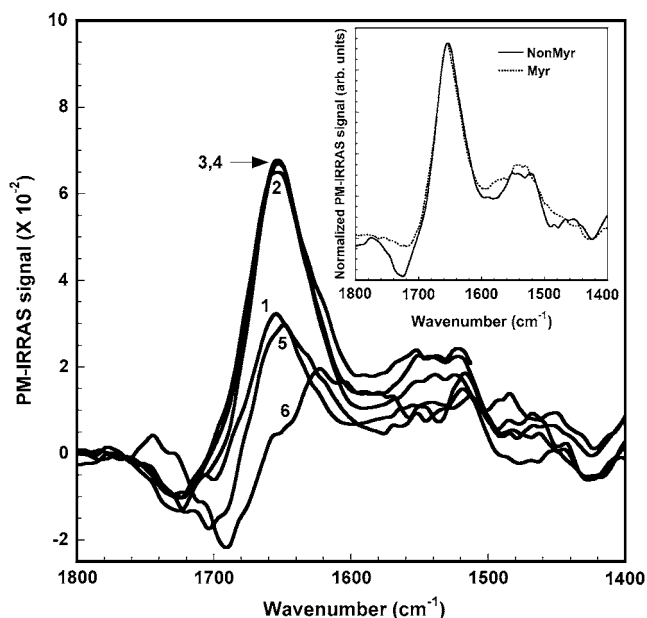
FIGURE 5 Typical PM-IRRAS spectra of nonmyristoylated recoverin during its adsorption onto a DMPC monolayer in the presence of calcium ($\Pi_0 = 5$ mN/m). Each PM-IRRAS spectrum was obtained during the 9 min of acquisition: spectra 1 (7.9–9 mN/m, 0–9 min), 2 (9–11.3 mN/m, 10–18 min), 3 (11.3–12 mN/m, 19–27 min), 4 (12–12.5 mN/m; 28–36 min), 5 (12.5–12.7 mN/m, 37–45 min), and 6 (12.7–12.8 mN/m, 46–54 min). The subphase and the concentration of recoverin was the same as in Fig. 3. (*Inset*) Normalized spectra 4 from myristoylated (*Myr*) (Fig. 3) and nonmyristoylated (*NonMyr*) recoverin (this figure). These measurements were performed with a polarizer positioned in front of the detector as described earlier (62). These data are representative of two independent experiments.

of the intensity of the amide I band could be explained by a dissociation of nonmyristoylated recoverin bound to the phospholipid monolayer. Since the surface pressure at the end of the adsorption of nonmyristoylated recoverin remains

stable beyond 1000 s of adsorption (data not shown), a possible dissociation of nonmyristoylated recoverin from the monolayer cannot explain the observed decrease in the PM-IRRAS signal (Fig. 6). Normalized spectra 3, 5, and 6 from Fig. 5 presented in Fig. 7 allow us to better visualize what is happening at large extents of adsorption of nonmyristoylated recoverin. First, the small shift of the amide I band of spectrum 5 compared to spectrum 3 could be due to the presence of the negative infrared band at $\sim$1690–1700 cm^{-1} in spectrum 5, which could partly originate from an improper subtraction of the DMPC monolayer because the orientation of the carbonyl groups of DMPC could have changed upon adsorption of nonmyristoylated recoverin. Second, it can be seen that the amide I band of nonmyristoylated recoverin shifts to lower frequencies in spectrum 6 compared to spectra 3 and 5, thus suggesting that large changes in secondary structure and/or in orientation of nonmyristoylated recoverin take place. However, given that we did not observe an increase of the intensity of the amide II band at the expense of the amide I band (44), an important change of orientation during the adsorption of nonmyristoylated recoverin can be excluded. Moreover, it is interesting to compare these data (Figs. 5 and 7) with those of nonmyristoylated recoverin when adsorbed alone (in the absence of the DMPC monolayer) at the air-water interface. Indeed, as shown in Fig. 8, nonmyristoylated recoverin does not behave the same in the presence (Fig. 5) and in the absence (Fig. 8) of a phospholipid monolayer. In fact, no decrease of the amide I intensity can be seen at large extents of adsorption (Fig. 8), which is very different from what has been observed in the presence of a DMPC monolayer (Figs. 5–7).

The refractive index of a protein at the air/water interface must be sufficiently different from that of water to allow its detection. Indeed, it has previously been observed that the adsorption of polylysine onto phospholipid monolayers
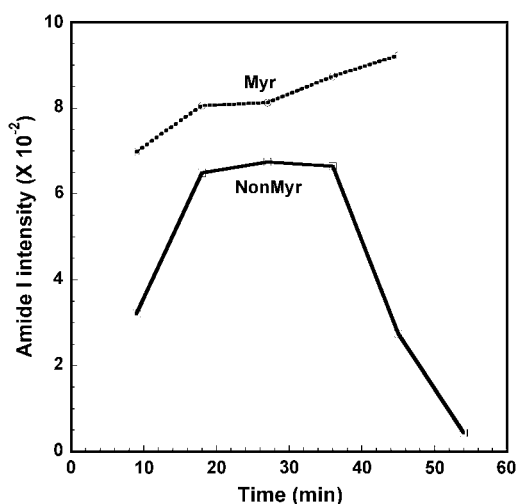

FIGURE 6 Intensity of the amide I band as a function of time during monolayer adsorption of myristoylated (*Myr*) (Fig. 3) and nonmyristoylated (*NonMyr*) recoverin (Fig. 5) on a water subphase in the presence of calcium.
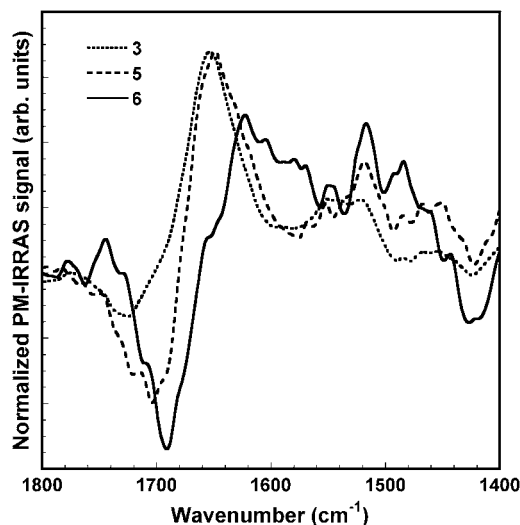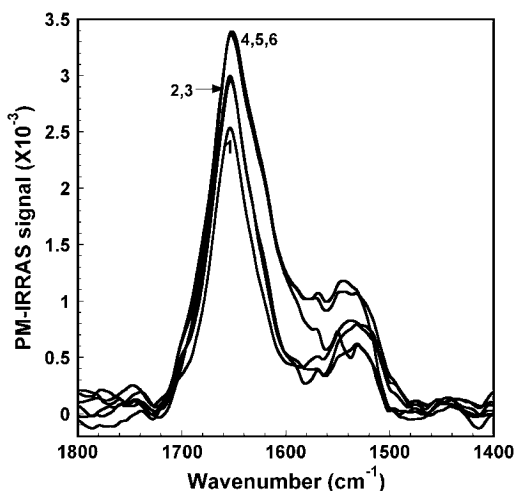

FIGURE 7 Normalized spectra 3–6 from Fig. 5.

FIGURE 8 Typical PM-IRRAS spectra of nonmyristoylated recoverin in the presence of calcium during its adsorption at the air-water interface (in the absence of a phospholipid monolayer). Each PM-IRRAS spectrum was obtained during the 9 min of acquisition: spectra 1 (0.7–2 mN/m, 0–9 min), 2 (2–3 mN/m, 10–18 min), 3 (4–6 mN/m, 19–27 min), 4 (9.5 mN/m, 28–36 min), 5 (9.6 mN/m, 37–45 min), and 6 (9.7 mN/m, 46–54 min). The subphase was the same as in Fig. 3. The final concentration of recoverin was 100 nM. These data are representative of three independent measurements.
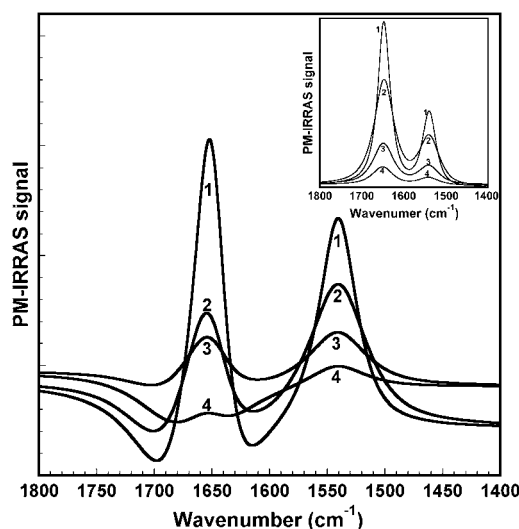

FIGURE 9 Simulation of the effect of different parameters on the spectrum of polybenzylglutamate on a water subphase: increase of the bandwidth from 40 (spectrum 1) to 60 cm^{-1} (spectrum 2); increase of protein hydration to 50% with a bandwidth of 60 cm^{-1} (spectrum 3); and 50% dielectric water with a bandwidth of 60 cm^{-1} (spectrum 4). (*Inset*) Simulation of the effect of different parameters on the spectrum of polybenzylglutamate on a D$_2$O subphase: increase of the bandwidth from 40 (spectrum 1) to 60 cm^{-1} (spectrum 2); increase of protein hydration to 50% with D$_2$O using a bandwidth of 60 cm^{-1} (spectrum 3); and 50% dielectric D$_2$O with a bandwidth of 60 cm^{-1} (spectrum 4).

leads to an increase of surface pressure which then remains stable. However, polylysine could not be detected by PM-IRRAS even though its amide bands could be clearly observed in ATR films (77). Polylysine is positively charged and thus highly hydrated. It can thus be postulated that the decrease of the intensity of the amide I band of nonmyristoylated recoverin could be due to a progressive hydration of this protein after 36 min adsorption which would result in an increase of its volume and a consequent dilution of the material at the surface. In this regard, we have performed simulations of the amide I and II bands of polybenzylglutamate (PBG) to find out the effect of different parameters on the intensity of these bands (see Fig. 9). The increase of the bandwidth from 40 to 60 cm^{-1} leads to a large decrease of the intensity of the amide I band (compare spectra 1 and 2, Fig. 9). Moreover, when hydrating PBG with 50% water, a further decrease of the amide I band can be seen (spectrum 3, Fig. 9). We have then performed an additional simulation to take into account the dielectric effect. Indeed, for diluted solutions, the corrected intensity of the amide I band, I_{cor}, is related to the observed intensity, I_{obs}, as described by Akiyama (78),

$$I_{cor} = \frac{9n_s}{\left(n_s^2 - k_s^2 + 2\right)^2 + 4n_s^2 k_s^2} I_{obs},\tag{4}$$

where n_s and k_s correspond to the refractive indices of the solvent. It can be seen that the amide I band almost vanishes completely when this correction is applied (spectrum 4, Fig. 9). Altogether, it can be postulated that from 36 min of adsorption, nonmyristoylated recoverin changes conforma-

tion and becomes progressively more hydrated, which leads to a loss of the infrared signal. In contrast, the myristoyl moiety of recoverin obviously allows stronger membrane binding, which leads to a highly oriented and organized myristoylated recoverin bound to the phospholipid monolayer.

To the author's knowledge, the only study regarding the structure of recoverin in interaction with a phospholipid model membrane is the NMR measurement of myristoylated recoverin in aligned bicelles (67). They have shown that the structure of myristoylated recoverin bound to bicelles is very similar to that in solution whereas we have observed a small change in secondary structure for recoverin bound onto phospholipid monolayers. Valentine et al. (67) did not study the structure of nonmyristoylated recoverin in aligned bicelles that could have shown a different dynamics or orientation when compared to myristoylated recoverin. It is noteworthy that it was not possible to obtain spectra of recoverin when injected beneath a DMPC monolayer at initial surface pressures >10 mN/m. To overcome this limitation we have used a D$_2$O subphase.

Monitoring of the adsorption of recoverin onto DMPC monolayers by PM-IRRAS spectroscopy using a D$_2$O subphase

To obtain PM-IRRAS spectra of recoverin at initial monolayer surface pressures higher than 5 mN/m, we have used a D$_2$O subphase to abolish the contribution of bulk water and

water vapor absorption to the PM-IRRAS signal in the region where recoverin absorption bands are observed. In addition, the refractive index of D_2O is different from that of water, which results in a greater mismatch between the film at the air/water interface and the subphase, thus allowing a better detection of the amide I band of proteins (40). Fig. 10 shows a typical spectrum of myristoylated recoverin bound to the DMPC monolayer using a D_2O subphase after a certain extent of adsorption. It can be seen that the amide I' band is better defined when compared to the spectrum measured on a water subphase (compare Fig. 10 with Fig. 3). The amide I' band is centered on 1643 cm^{-1}, which may look unusual for α-helices. However, this position is in good agreement with the FTIR spectrum of recoverin measured between CaF_2 plates in D_2O buffer where the amide I' band was centered at 1644 cm^{-1} (79). Moreover, the position of the amide I band of recoverin is shifted by 11 cm^{-1} (1655 to 1644 cm^{-1}) on the D_2O subphase compared to the water subphase, thus indicating an elevated hydrogen-deuterium exchange of the peptide moiety of recoverin. Similar shifts of the frequency of the amide I band in the presence of D_2O have been observed for several EF-hand calcium-binding proteins using FTIR spectroscopy (i.e., calmodulin, troponin C, and parvalbumin), which are homologous to recoverin (80,81). This phenomenon has been explained by a high degree of solvent interaction (80). Moreover, a shift of 12 cm^{-1} of the amide I band was also observed for α-helical peptides studied at the air/D_2O interface using IRRAS (76). These observations are also consistent with the large amount
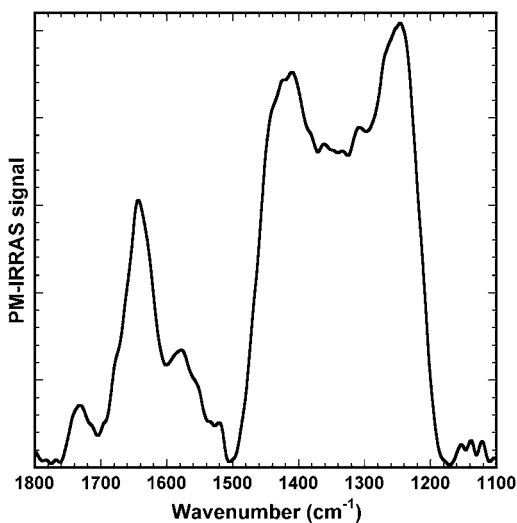

FIGURE 10 Typical PM-IRRAS spectrum of myristoylated recoverin bound onto a DMPC monolayer in presence of calcium using a D_2O subphase. The initial surface pressure of the phospholipid monolayer was 5 mN/m. The spectrum was recorded during the adsorption of myristoylated recoverin within a range of 5–14 mN/m of surface pressure change. The subphase was 1 mM HEPES, pD 7.9, 100 mM NaCl, 1 mM $CaCl_2$ (pD = pH + 0.4). The final concentration of recoverin was 50 nM. These data are representative of five independent experiments.

of α-helical structure in recoverin. In addition, two other components are present in the amide I' band of the spectrum shown in Fig. 10. The shoulders at 1630 cm^{-1} and ~1678 cm^{-1} can been assigned to β-sheet and β-turn structures of recoverin, respectively (40,51,76,82). Indeed, Johnson et al. (83) have shown that recoverin in the presence of 1 mM calcium contains 11% parallel and antiparallel β-sheet and 13% of β-turn. In addition, the NMR analysis of the secondary structure of recoverin revealed the presence of 11 helical segments and two pairs of antiparallel β-sheets (31). The D_2O subphase allows the observation of a broad band centered at 1570 cm^{-1}, which corresponds to the COO^- antisymmetric stretching band of glutamic acid present at the last position of the EF-hand loops as previously demonstrated by Ozawa et al. (79) using FTIR spectroscopy. It is noteworthy that the strong and broad band below 1500 cm^{-1} corresponds to the δ(HOD) mode and must not be assigned to a not completely exchanged amide II band (see Fig. 10). Indeed, the HOD molecules have been presumably formed in the presence of H_2O vapor in our chamber, which accumulates with time at the interface and in the subphase. Such an attribution of this band has also been suggested by Ulrich and Vogel (84). This possibility was further tested by recording spectra of the free subphase in the same conditions. The recorded spectra clearly showed an increase of this broad band below 1500 cm^{-1} with time (data not shown).

The adsorption of myristoylated and nonmyristoylated recoverin onto phospholipid monolayers has thus been monitored at a higher initial surface pressure of 15 mN/m (compared to Fig. 3) using the D_2O subphase. In these conditions, the adsorption of myristoylated and nonmyristoylated recoverin onto a DMPC monolayer led to a surface pressure increase from 15 to 19 mN/m. After 9 min of adsorption, the intensity of the amide I' band of myristoylated recoverin (Fig. 11) is stronger than that of the nonmyristoylated protein (Fig. 12). Moreover, the intensity of the amide I' band of nonmyristoylated recoverin is markedly reduced in the spectra measured after 18 and 27 min of adsorption (spectra 2 and 3, respectively, Fig. 12) whereas the intensity of myristoylated recoverin remains almost unchanged for all recorded spectra (Figs. 11 and 13). This observation is similar to that observed at lower initial surface pressure (Fig. 6). However, at a higher initial surface pressure, the conformation of nonmyristoylated recoverin remains unchanged which contrasts with the behavior observed at lower initial surface pressure (compare spectrum 6 in Fig. 5 with spectrum 3 in Fig. 12) although longer extents of adsorption could have led to similar results. Simulations of the amide I region of PBG with D_2O have also been performed to find out the effect of different parameters on the intensity of these bands (see *inset* of Fig. 9). As observed with water (Fig. 9), a bandwidth increase from 40 to 60 cm^{-1} leads to a large decrease of the intensity of the amide I band (compare spectra 1 and 2, *inset* of Fig. 9). Moreover, a further decrease of the amide I band intensity can be seen when hydrating PBG with 50% D_2O and
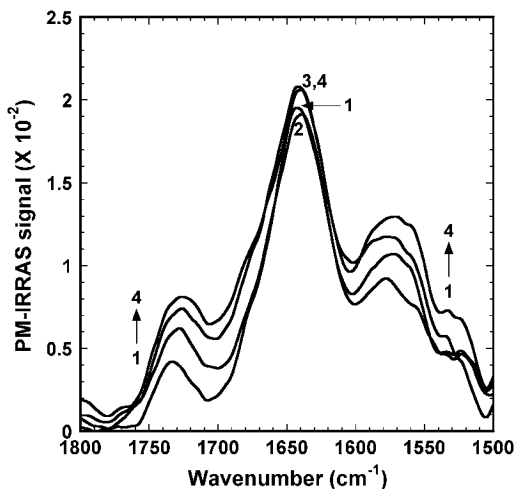
FIGURE 11 Typical PM-IRRAS spectra of myristoylated recoverin during its adsorption onto a DMPC monolayer in presence of calcium using a D_2O subphase. Each PM-IRRAS spectrum was obtained during the 9 min of acquisition: spectra 1 (15–19.4 mN/m, 0–9 min); 2 (19.4 mN/m, 10–18 min); 3 (19.3 mN/m, 19–27 min); and 4 (19.3 mN/m, 28–36 min). Conditions are the same as Fig. 10. These data are representative of two independent measurements.

FIGURE 13 Intensity of the amide I' band as a function of time during monolayer adsorption of myristoylated (*Myr*) (Fig. 11) and nonmyristoylated (*NonMyr*) recoverin (Fig. 12) on a D_2O subphase in the presence of calcium.

50% dielectric D_2O, (spectra 3 and 4, respectively, *inset* of Fig. 9). In contrast to the simulations using H_2O (Fig. 9), the intensity of the amide I band does not vanish to almost 0 with 50% dielectric D_2O (*inset* of Fig. 9), which is consistent with the experimental observations. Altogether, these results strongly suggest that the myristoyl moiety is necessary to allow a stable binding of recoverin onto phospholipid monolayers. Furthermore, it can be postulated that nonmyristoylated recoverin is more solvated because of a weaker
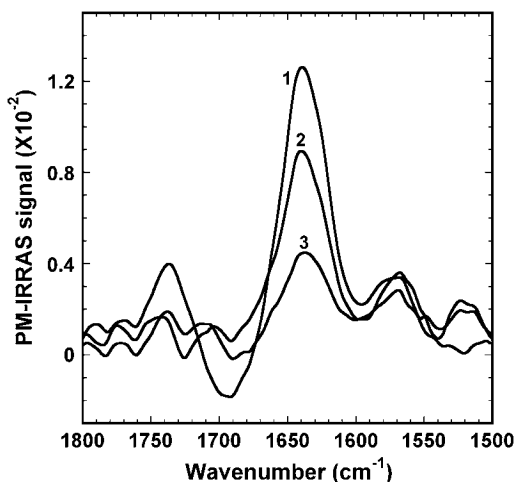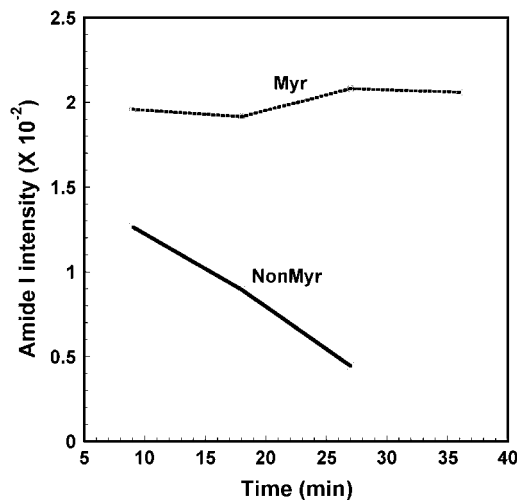
interaction with phospholipid monolayers. Therefore, during the short recovery of phototransduction where calcium concentration comes back to the dark level, recoverin must quickly inactivate the membrane-bound rhodopsin kinase, thereby allowing rhodopsin to reenter in its active state. Such a quick action of recoverin could be enabled by its myristoyl group, in addition to hydrophobic amino acids, as demonstrated in the present article. Indeed, its myristoyl group, in particular, should provide a favorable orientation and a fast binding and targeting of recoverin to photoreceptor disk membranes, thus allowing it to efficiently bind and inactivate rhodopsin kinase. Conversely, the fall in calcium concentration after photoreceptor light activation results in the sequestration of the myristoyl group of recoverin in a hydrophobic cleft. The present observations of a much slower kinetics of binding of recoverin in the absence of calcium should result in its improper membrane binding and, consequently, in the activation of rhodopsin kinase.

Effect of zinc on recoverin adsorption in monolayers and on its limited proteolysis

Retina contains high amounts of zinc and its localization in photoreceptors varies after light activation of phototransduction (for a review, see (85)). Moreover, it has been shown that several proteins in photoreceptors bind zinc ions such as rhodopsin (86), phosphodiesterase (87) and, more recently, recoverin (33). The adsorption of myristoylated recoverin onto phospholipid monolayers has thus been measured in the presence of zinc and compared to the effect of calcium. Fig. 14 *A* shows a histogram of the surface pressure increase ($\Delta\Pi$) upon myristoylated and nonmyristoylated recoverin adsorption onto phospholipid monolayers at an initial pressure (Π_0) of 10 mN/m in the presence of calcium or

FIGURE 12 Typical PM-IRRAS spectra of nonmyristoylated recoverin during its adsorption onto a DMPC monolayer in presence of calcium using a D_2O subphase. Each PM-IRRAS spectrum was obtained during the 9 min of acquisition: spectra 1 (15–19 mN/m, 0–9 min); 2 (19.1–19.3 mN/m, 10–18 min); and 3 (19.3 mN/m, 19–27 min). Conditions are the same as Fig. 10. These data are representative of two independent measurements.
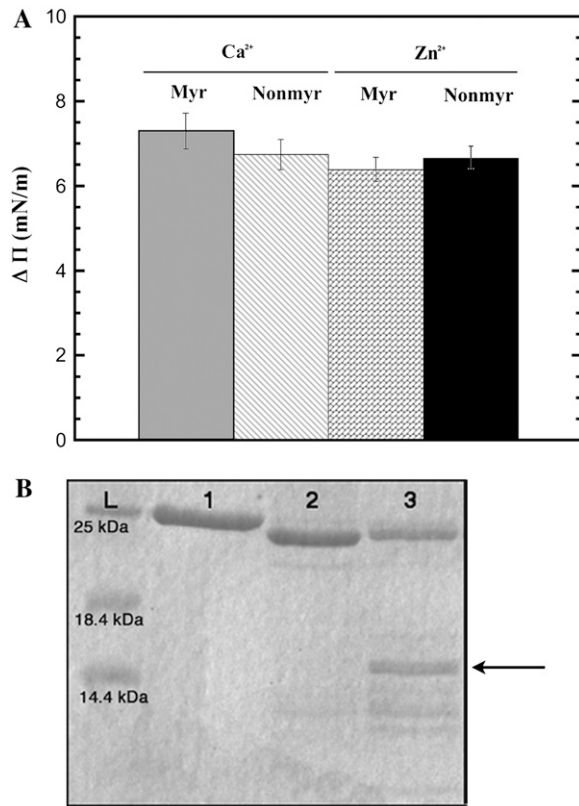
FIGURE 14   (*A*) Histogram of the surface pressure increase ($\Delta\Pi$) upon myristoylated and nonmyristoylated recoverin adsorption onto a DMPC monolayer at an initial pressure of 10 mN/m in the presence of calcium or zinc. The subphase was 1 mM HEPES, pH 7.5, 100 mM NaCl, 1 mM $CaCl_2$, or 1 mM $ZnCl_2$. The final concentration of recoverin was 50 nM. The error bar is the standard deviation calculated from three independent measurements for each individual experimental condition assayed. (*B*) SDS-PAGE gel electrophoresis of the undigested myristoylated recoverin (lane 1) and of myristoylated recoverin after proteolysis by TPCK-trypsin in presence of calcium (lane 2) or zinc (lane 3). The lane (*L*) is the protein ladder.

zinc. It can be seen that the extent of adsorption of myristoylated and nonmyristoylated recoverin onto phospholipid monolayers in the presence of zinc is similar to that in the presence of calcium. These data suggest that calcium and zinc induce a similar conformational change of recoverin, which leads to similar extents of binding to phospholipid monolayers. To verify whether this conformational change of recoverin induced upon zinc binding is identical to that taking place in the presence of calcium, limited proteolysis of recoverin by trypsin was performed. Fig. 14 *B* shows the SDS-PAGE electrophoresis after 15 min proteolysis of myristoylated recoverin by TPCK-trypsin in the presence of calcium or zinc. In the presence of calcium (lane 2), hydrolyzed recoverin appears as a main band at a position slightly lower than the native, undigested recoverin (lane 1). Two additional minor bands are also present, indicating a cleavage of two short peptides of recoverin by trypsin. This pattern is identical to the previous results obtained by Dizhoor et al. (19). In fact, they have shown that

trypsin removes the COOH-terminal (Lys^{194}-Leu^{202}) as well as the NH_2 terminal myristoyl moiety (myristoyl-Lys^5) of recoverin in the presence of calcium. However, in the presence of zinc (lane 3), multiple hydrolyzed products of myristoylated recoverin can be seen which are different from those observed in the presence of calcium (lane 2). In fact, the intensity of the bands indicate that a larger amount of recoverin is cleaved after 15 min in the presence of zinc (lane 3) compared to hydrolysis in the presence of calcium (lane 2). Moreover, a cleaved fragment of ~15 kDa (see *arrow*, lane 3) appeared in this condition. These results indicate that zinc-bound recoverin has trypsic sites that are different from those of the calcium-bound recoverin. Furthermore, these data suggest that a different conformational change of recoverin in the presence of zinc compared to calcium is responsible for its adsorption onto phospholipid monolayers although comparable extents of adsorption are obtained. This conclusion is in agreement with previous results of Permyakov et al. (33), who have shown that a double mutant of recoverin where calcium binding sites are inactivated can still bind zinc ions. Moreover, they have demonstrated that zinc decreases the thermal stability of recoverin. In addition, the effect of zinc, in addition to other ions, must be taken into account to improve our understanding of the modulation of recoverin membrane binding during phototransduction.

CONCLUSIONS

Altogether, the present data shows that myristoylated recoverin binds model membranes much faster than non-myristoylated recoverin. In addition, the myristoyl moiety favors proper orientation and stable membrane binding of recoverin in contrast to the nonmyristoylated protein which becomes hydrated, disorganized, and disordered after membrane binding. Highly polyunsaturated fatty acyl chains of photoreceptors and electrostatic components are also important parameters in recoverin membrane binding (to be published elsewhere).

REFERENCES

1. Kinnunen, P. K. J., A. Kõiv, J. Y. A. Lehtonen, M. Rytömaa, and P. Mustonen. 1994. Lipid dynamics and peripheral interactions of proteins with membrane surfaces. *Chem. Phys. Lipids.* 73:181–207.

2. Marsh, D., and T. Páli. 2004. The protein-lipid interface: perspectives from magnetic resonance and crystal structures. *Biochim. Biophys. Acta.* 1666:118–141.

3. Grenier, S., P. Desmeules, A. K. Dutta, A. Yamazaki, and C. Salesse. 1998. Determination of the depth of penetration of the α subunit of retinal G protein in membranes: a spectroscopic study. *Biochim. Biophys. Acta.* 1370:199–206.

4. Arbuzova, A., A. A. P. Schmitz, and G. Vergères. 2002. Cross-talk unfolded: MARKS proteins. *Biochem. J.* 362:1–12.

5. Desmeules, P., M. Grandbois, V. A. Bonderenko, A. Yamazaki, and C. Salesse. 2002. Measurement of membrane binding between recoverin, a calcium-myristoyl switch protein, and lipid bilayers by AFM-based force spectroscopy. *Biophys. J.* 82:3343–3350.

6. Meister, A., C. Nicolini, H. Waldmann, J. Kuhlmann, A. Kerth, R. Winter, and A. Blume. 2006. Insertion of lipidated Ras proteins into lipid monolayers studied by infrared reflection absorption spectroscopy (IRRAS). *Biophys. J.* 91:1388–1401.

7. Duronio, R. J., E. Jackson-Machelski, R. O. Heuckeroth, P. O. Olins, C. S. Devine, W. Yonemoto, L. W. Slice, S. S. Taylor, and J. I. Gordon. 1990. Protein *N*-myristoylation in *Escherichia coli*: reconstitution of a eukaryotic protein modification in bacteria. *Proc. Natl. Acad. Sci. USA.* 87:1506–1510.

8. Dunphy, J. T., and M. E. Linder. 1998. Signaling functions of protein palmitoylation. *Biochim. Biophys. Acta.* 1436:245–261.

9. Resh, M. D. 1999. Fatty acylation of proteins: new insights into membrane targeting of myristoylated and palmitoylated proteins. *Biochim. Biophys. Acta.* 1451:1–16.

10. Resh, M. D. 2004. Membrane targeting of lipid modified signal transduction proteins. *Subcell. Biochem.* 37:217–232.

11. McLaughlin, S., and A. Aderem. 1995. The myristoyl-electrostatic switch: a modulator of reversible protein-membrane interactions. *Trends Biochem. Sci.* 20:272–276.

12. Ames, J. B., and M. Ikura. 2002. Structure and membrane-targeting mechanism of retinal Ca^{2+}-binding proteins, recoverin and GCAP-2. *Adv. Exp. Med. Biol.* 514:333–348.

13. Ames, J. B., T. Tanaka, L. Stryer, and M. Ikura. 1996. Portrait of a myristoyl switch protein. *Curr. Opin. Struct. Biol.* 6:432–438.

14. Dizhoor, A. M., S. Ray, S. Kumar, G. Niemi, M. Spencer, D. Brolley, K. A. Walsh, P. P. Philipov, J. B. Hurley, and L. Stryer. 1991. Recoverin: a calcium sensitive activator of retinal rod guanylate cyclase. *Science.* 251:915–918.

15. Bazhin, A. V., D. Schadendorf, P. P. Philippov, and S. B. Eichmüller. 2006. Recoverin as a cancer-retina antigen. *Cancer Immunol. Immunother.* 56:110–116.

16. Ames, J. B., T. Tanaka, M. Ikura, and L. Stryer. 1995. Nuclear magnetic resonance evidence for Ca^{2+}-induced extrusion of the myristoyl group of recoverin. *J. Biol. Chem.* 270:30909–30913.

17. Flaherty, K. M., S. Zozulya, L. Stryer, and D. B. McKay. 1993. Three-dimensional structure of recoverin, a calcium sensor in vision. *Cell.* 75:709–716.

18. Burgoyne, R. D. 2004. The neuronal calcium-sensor proteins. *Biochim. Biophys. Acta.* 1742:59–68.

19. Dizhoor, A. M., L. H. Ericsson, R. S. Johnson, S. Kumar, E. Olshevskaya, S. Zozulya, T. A. Neubert, L. Stryer, J. B. Hurley, and K. A. Walsh. 1992. The NH_2 terminus of retinal recoverin is acylated by a small family of fatty acids. *J. Biol. Chem.* 267:16033–16036.

20. Dizhoor, A. M., C. K. Chen, E. Olshevskaya, V. V. Sinelnikova, P. Phillipov, and J. B. Hurley. 1993. Role of the acylated amino terminus of recoverin in Ca^{2+}-dependent membrane interaction. *Science.* 259:829–832.

21. Zozulya, S., and L. Stryer. 1992. Calcium-myristoyl protein switch. *Proc. Natl. Acad. Sci. USA.* 89:11569–11573.

22. Chen, C. K., J. Inglese, R. J. Lefkowitz, and J. B. Hurley. 1995. Ca^{2+}-dependent interaction of recoverin with rhodopsin kinase. *J. Biol. Chem.* 270:18060–18066.

23. Gray-Keller, M. P., A. S. Polans, K. Palczewski, and P. B. Detwiler. 1993. The effect of recoverin-like calcium-binding proteins on the photoresponse of retinal rods. *Neuron.* 10:523–531.

24. Kawamura, S., O. Hisatomi, S. Kayada, F. Tokunaga, and C. H. Kuo. 1993. Recoverin has S-modulin activity in frog rods. *J. Biol. Chem.* 268:14579–14582.

25. Klenchin, V. A., P. D. Calvert, and M. D. Bownds. 1995. Inhibition of rhodopsin kinase by recoverin. Further evidence for a negative feedback system in phototransduction. *J. Biol. Chem.* 270:16147–16152.

26. Senin, I. I., A. A. Zargarov, A. M. Alekseev, E. N. Gorodovikova, V. M. Lipkin, and P. P. Philippov. 1995. *N*-myristoylation of recoverin enhances its efficiency as an inhibitor of rhodopsin kinase. *FEBS Lett.* 376:87–90.

27. Makino, C. L., R. L. Dodd, J. Chen, M. E. Burns, A. Roca, M. I. Simon, and D. A. Baylor. 2004. Recoverin regulates light-dependent phosphodiesterase activity in retinal rods. *J. Gen. Physiol.* 123:729–741.

28. Ames, J. B., R. Ishima, T. Tanaka, J. I. Gordon, L. Stryer, and M. Ikura. 1997. Molecular mechanics of calcium-myristoyl switches. *Nature.* 389:198–202.

29. Hughes, R. E., P. S. Brzovic, R. E. Klevit, and J. B. Hurley. 1995. Calcium-dependent solvation of the myristoyl group of recoverin. *Biochemistry.* 34:11410–11416.

30. Desmeules, P. 2006. Overexpression and study of the parameters responsible for the binding of acylated proteins to membranes and optimization of recoverin myristoylation in *E. coli.* PhD thesis, Université du Québec à Trois-Rivières, Canada.

31. Ames, J. B., T. Tanaka, L. Stryer, and M. Ikura. 1994. Secondary structure of myristoylated recoverin determined by three-dimensional heteronuclear NMR: implications for the calcium-myristoyl switch. *Biochemistry.* 33:10743–10753.

32. Tanaka, T., J. B. Ames, T. S. Harvey, L. Stryer, and M. Ikura. 1995. Sequestration of the membrane-targeting myristoyl group of recoverin in the calcium-free state. *Nature.* 376:444–447.

33. Permyakov, S. E., A. M. Cherskaya, L. A. Wasserman, T. I. Khoklova, I. I. Senin, A. A. Kargarov, D. V. Zinchenko, E. Y. Zernii, V. M. Lipkin, P. P. Philippov, V. N. Uversky, and E. A. Permyakov. 2003. Recoverin is a zinc-binding protein. *J. Proteome Res.* 2:51–57.

34. Peitzsch, R. M., and S. McLaughlin. 1993. Binding of acylated peptides and fatty acids to phospholipid vesicles: pertinence to myristoylated proteins. *Biochemistry.* 32:10436–10443.

35. Pool, C. T., and T. E. Thompson. 1998. Chain length and temperature dependence of the reversible association of model acylated proteins with lipid bilayers. *Biochemistry.* 37:10246–10255.

36. Murray, D., N. Ben-Tal, B. Honig, and S. McLaughlin. 1997. Electrostatic interaction of myristoylated recoverin with membranes: simple physics, complicated biology. *Structure.* 15:985–989.

37. Silvius, J. R., and M. J. Zuckermann. 1993. Interbilayer transfer of phospholipid-anchored macromolecules via monomer diffusion. *Biochemistry.* 32:3153–3161.

38. Finkelstein, A. V., and J. Janin. 1989. The price of lost freedom: entropy of bimolecular complex formation. *Protein Eng.* 3:1–3.

39. Dynarowicz-Latka, P., A. Dhanabalan, and O. N. Oliveira, Jr. 2001. Modern physicochemical research on Langmuir monolayers. *Adv. Colloid Interface Sci.* 91:221–293.

40. Mendelsohn, R., and C. R. Flach. 2002. Infrared reflection-absorption spectroscopy of lipids, peptides, and protein in aqueous monolayers. *In* Current Topics in Membranes: Peptide-Lipid Interaction, Vol. 52. S. A. Simon and T. J. McIntosh, editors. Academic Press, New York.

41. Heitz, F., and N. Van Mau. 2002. Protein structural changes induced by their uptake at interfaces. *Biochim. Biophys. Acta.* 1597:1–11.

42. Buffeteau, T., B. Desbat, and J. M. Turlet. 1991. Polarization modulation FT-IR spectroscopy of surfaces and ultra-thin films: experimental procedure and quantitative analysis. *Appl. Spectrosc.* 45:380–389.

43. Blaudez, D., T. Buffeteau, J. C. Cornut, B. Desbat, N. Escafre, and M. Pézolet. 1994. Polarization modulation FTIR spectroscopy at the air-water interface. *Thin Solid Films.* 242:146–150.

44. Cornut, I., B. Desbat, J.-M. Turlet, and J. Dufourcq. 1996. In situ study by polarization modulated Fourier transform infrared spectroscopy of the structure and orientation of lipids and amphipathic peptides at the air-water interface. *Biophys. J.* 70:305–312.

45. Flach, C. R., F. G. Prendergast, and R. Mendelsohn. 1996. Infrared reflection-absorption of melittin interaction with phospholipid monolayers at the air/water interface. *Biophys. J.* 70:539–546.

46. Gallant, J., B. Desbat, D. Vaknin, and C. Salesse. 1998. Polarization-modulated infrared spectroscopy and x-ray reflectivity of photosystem II core complex at the gas-water interface. *Biophys. J.* 75:2888–2899.

47. Bellet-Amalric, E., D. Blaudez, B. Desbat, F. Graner, F. Gauthier, and A. Renault. 2000. Interaction of the third helix of *Antennapedia* homeodomain and a phospholipid monolayer, studied by ellipsometry and PM-IRRAS at the air-water interface. *Biochim. Biophys. Acta.* 1467:131–143.

48. Castano, S., B. Desbat, and J. Dufourcq. 2000. Ideally amphipathic β-sheeted peptides at interfaces: structure, orientation, affinities for lipids and hemolytic activity of KLmK peptides. *Biochim. Biophys. Acta.* 1463:65–80.

49. Castano, S., B. Desbat, M. Laguerre, and J. Dufoucq. 1999. Structure, orientation and affinity for interfaces and lipids of ideally amphipathic lytic L_iK_j (*i*=2*j*) peptides. *Biochim. Biophys. Acta.* 1416: 176–194.

50. Castano, S., D. Blaudez, B. Desbat, J. Dufourcq, and H. Wróblewski. 2002. Secondary structure of spiralin in solution, at the air/water interface, and in interaction with lipid monolayers. *Biochim. Biophys. Acta.* 1562:45–56.

51. Lavoie, H., B. Desbat, D. Vaknin, and C. Salesse. 2002. Structure of rhodopsin in monolayers at the air-water interface: a PM-IRRAS and x-ray reflectivity study. *Biochemistry.* 41:13424–13434.

52. Wu, F., A. Gericke, C. R. Flach, T. R. Mealy, B. A. Seaton, and R. Mendelsohn. 1998. Domain structure and molecular conformation in annexin V/1,2-dimyristoyl-*sn*-glycero-3 phosphate/Ca^{2+} aqueous monolayers: a Brewster angle microscopy/infrared reflection absorption spectroscopy study. *Biophys. J.* 74:3273–3281.

53. Gericke, A., and H. Hühnerfuss. 1994. IR reflection absorption spectroscopy: a versatile tool for studying interfacial enzymatic processes. *Chem. Phys. Lipids.* 74:205–210.

54. Grandbois, M., B. Desbat, D. Blaudez, and C. Salesse. 1999. Polarization-modulated infrared absorption spectroscopy measurement of phospholipid monolayer hydrolysis by phospholipase C. *Langmuir.* 15:6594–6597.

55. Grandbois, M., B. Desbat, and C. Salesse. 2000. Monitoring of phospholipid monolayer hydrolysis by phospholipase A2 by use of polarization-modulated Fourier transform infrared spectroscopy. *Biophys. Chem.* 88:127–135.

56. Wang, X., S. Zheng, Q. He, G. Brezesinski, H. Möhwald, and J. Li. 2005. Hydrolysis reaction analysis of L-α-distearoylphosphatidylcholine monolayer catalyzed by phospholipase A_2 with polarization-modulated infrared reflection absorption spectroscopy. *Langmuir.* 21:1051–1054.

57. Ray, S., S. Zozulya, G. A. Niemi, K. M. Flaherty, D. Brolley, A. M. Dizhoor, D. B. McKay, J. B. Hurley, and L. Stryer. 1992. Cloning, expression, and crystallization of recoverin, a calcium sensor in vision. *Proc. Natl. Acad. Sci. USA.* 89:5705–5709.

58. Desmeules, P., S.-E. Penney, and C. Salesse. 2006. Single-step purification of myristoylated and nonmyristoylated recoverin and substrate dependence of myristoylation level. *Anal. Biochem.* 349:25–32.

59. Bradford, M. M. 1976. A rapid and sensitive method for the quantitation of microgram quantities of protein utilizing the principle of protein-dye binding. *Anal. Biochem.* 72:248–254.

60. Pitcher III, W. H., S. L. Keller, and W. H. Huestis. 2002. Interaction of nominally soluble proteins with phospholipid monolayers at the air-water interface. *Biochim. Biophys. Acta.* 154:107–113.

61. Blaudez, D., J.-M. Turlet, J. Dufourcq, D. Bard, T. Buffeteau, and B. Desbat. 1996. Investigation at the air/water interface using polarization modulation IR spectroscopy. *J. Chem. Soc. Faraday Trans.* 92:525–530.

62. Saccani, J., T. Buffeteau, B. Desbat, and B. D. Saccani. 2003. Increasing detectivity of polarization modulation infrared reflection-absorption spectroscopy for the study of ultrathin films deposited on various substrates. *Appl. Spectrosc.* 57:1260–1265.

63. Buffeteau, T., and B. Desbat. 1989. Thin-film optical constants determined from infrared reflectance and transmittance measurements. *Appl. Spectrosc.* 43:1027–1032.

64. Berreman, D. W. 1972. Optics in stratified and anisotropic media: 4 × 4-matrix formulation. *J. Opt. Soc. Am.* 62:502–510.

65. Bertie, J. E., and Z. Lan. 1996. Infrared intensities of liquids. XX. The intensity of the OH stretching band of liquid water revisited, and the best current values of the optical constants of $H_2O(l)$ at 25°C between 15,000 and 1 cm^{-1}. *Appl. Spectrosc.* 50:1047–1057.

66. Buffeteau, T., E. Le Calvez, S. Castano, B. Desbat, D. Blaudez, and J. Dufourcq. 2000. Anisotropic optical constants of α-helix and β-sheet secondary structures in the infrared. *J. Phys. Chem. B.* 104: 4537–4544.

67. Valentine, K. G., M. F. Mesleh, S. J. Opella, M. Ikura, and J. B. Ames. 2003. Structure, topology and dynamics of myristoylated recoverin bound to phospholipids bilayers. *Biochemistry.* 42:6334–6340.

68. Kataoka, M., K. Mihara, and F. Tokunaga. 1993. Recoverin alters its surface properties depending on both calcium-binding and N-terminal myristoylation. *J. Biochem. (Tokyo).* 114:535–540.

69. Cho, D., G. Narsimhan, and E. I. Franses. 1997. Adsorption dynamics of native and pentylated bovine serum albumin at air-water interfaces: surface concentration/surface pressure measurements. *J. Colloid Interface Sci.* 191:312–325.

70. Xia, X.-F., F. Wang, and S.-F. Sui. 2001. Effect of phospholipid on trichosanthin adsorption at the air-water interface. *Biochim. Biophys. Acta.* 1515:1–11.

71. Wierenga, P. A., M. B. J. Meinders, M. R. Egmond, F. A. G. J. Voragen, and H. H. de Jongh. 2003. Protein exposed hydrophobicity reduces the kinetic barrier for adsorption of ovalbumin to the air-water interface. *Langmuir.* 19:8964–8970.

72. Lange, C., and K. W. Koch. 1997. Calcium-dependent binding of recoverin to membranes monitored by surface plasmon resonance spectroscopy in real time. *Biochemistry.* 36:12019–12026.

73. Dousseau, F., and M. Pézolet. 1990. Determination of the secondary structure content of proteins in aqueous solutions from their amide I and amide II infrared bands. Comparison between classical and partial least-squares methods. *Biochemistry.* 29:8771–8779.

74. Surewicz, W. K., H. H. Mantsch, and D. Chapman. 1993. Determination of protein secondary structure by Fourier transform infrared spectroscopy: a critical assessment. *Biochemistry.* 32:389–394.

75. Goormaghtigh, E., V. Cabiaux, and J.-M. Ruysschaert. 1994. Determination of soluble and membrane protein structure by Fourier transform infrared spectroscopy. *In* Subcellular Biochemistry: Physicochemical Methods in the Study of Biomembranes, Vol. 23. H. J. Hildelson and G. B. Ralston, editors. Plenum Press, New York.

76. Flach, C. R., J. W. Brauner, J. W. Taylor, R. C. Baldwin, and R. Mendelsohn. 1994. External reflection FTIR of peptide monolayer films in situ at the air/water interface: experimental design, spectra-structure correlations and effects of hydrogen-deuterium exchange. *Biophys. J.* 67:402–410.

77. Labrecque, J. 1995. Infrared spectroscopic study of the interaction of polylysine with phosphatidic acid in monolayers. MSc thesis, Université Laval, Québec, Canada.

78. Akiyama, M. 1984. Internal field correction for infrared band intensity measured in solutions. *J. Chem. Phys.* 81:5229–5230.

79. Ozawa, T., M. Fukuda, M. Nara, A. Nakamura, Y. Komine, K. Kohama, and Y. Umezawa. 2000. How can Ca^{2+} selectively activate recoverin in the presence of Mg^{2+}? Surface plasmon resonance and FTIR spectroscopic studies. *Biochemistry.* 39:14495–14503.

80. Jackson, M., P. I. Haris, and D. Chapman. 1991. Fourier transform infrared spectroscopic studies of Ca^{2+} binding proteins. *Biochemistry.* 30:9681–9686.

81. Trewhella, J., W. K. Liddle, D. B. Heidorn, and N. Strynadka. 1989. Calmodulin and troponin C structures studied by Fourier transform infrared spectroscopy: effects of Ca^{2+} and Mg^{2+} binding. *Biochemistry.* 28:1294–1301.

82. Surewicz, W. K., and H. H. Mantsch. 1988. New insight into protein secondary structure from resolution-enhanced infrared spectra. *Biochim. Biophys. Acta.* 952:115–130.

83. Johnson, W. C., Jr., K. Palczewski, W. A. Gorczyca, J. H. Riazance-Lawrence, D. Witkowska, and A. S. Polans. 1997. Calcium binding to recoverin: implication for secondary structure and membrane association. *Biochim. Biophys. Acta.* 1342:164–174.

84. Ulrich, W.-P., and H. Vogel. 1999. Polarization-modulated FTIR spectroscopy of lipid/gramicidin monolayers at the air/water interface. *Biophys. J.* 76:1639–1647.

85. Ugarte, M., and N. N. Osborne. 2001. Zinc in the retina. *Prog. Neurobiol.* 64:219–249.

86. Shuster, T. A., A. K. Nagy, D. C. Conly, and D. B. Farber. 1992. Direct zinc binding to purified rhodopsin and disc membranes. *Biochem. J.* 282:123–128.

87. Francis, S. H., J. L. Colbran, L. M. McAllister-Lucas, and J. D. Corbin. 1994. Zinc interaction and conserved motifs of the cGMP-binding cGMP-specific phosphodiesterase suggest that it is a zinc hydrolase. *J. Biol. Chem.* 269:22477–22480.